REPORT DOCUMENTATION PAGE

Form Approved
OMB No. 0704-0188

1. REPORT DATE *(DD-MM-YYYY)*	2. REPORT TYPE	3. DATES COVERED *(From - To)*
	Technical Papers	

4. TITLE AND SUBTITLE

5a. CONTRACT NUMBER

5b. GRANT NUMBER

5c. PROGRAM ELEMENT NUMBER

6. AUTHOR(S)

5d. PROJECT NUMBER
1011

5e. TASK NUMBER
CA9F

5f. WORK UNIT NUMBER

7. PERFORMING ORGANIZATION NAME(S) AND ADDRESS(ES)

Air Force Research Laboratory (AFMC)
AFRL/PRS
5 Pollux Drive
Edwards AFB CA 93524-7048

8. PERFORMING ORGANIZATION REPORT

9. SPONSORING / MONITORING AGENCY NAME(S) AND ADDRESS(ES)

Air Force Research Laboratory (AFMC)
AFRL/PRS
5 Pollux Drive
Edwards AFB CA 93524-7048

10. SPONSOR/MONITOR'S ACRONYM(S)

11. SPONSOR/MONITOR'S NUMBER(S)

12. DISTRIBUTION / AVAILABILITY STATEMENT

Approved for public release; distribution unlimited.

13. SUPPLEMENTARY NOTES

14. ABSTRACT

15. SUBJECT TERMS

16. SECURITY CLASSIFICATION OF:			17. LIMITATION OF ABSTRACT	18. NUMBER OF PAGES	19a. NAME OF RESPONSIBLE PERSON
a. REPORT	b. ABSTRACT	c. THIS PAGE			Leilani Richardson
Unclassified	Unclassified	Unclassified	A		19b. TELEPHONE NUMBER *(include area code)* (661) 275-5015

18 separate items enclosed

U

10119QF

TP-1998-078

MEMORANDUM FOR PRS (Contractor Publication)

FROM: PROI (TI) (STINFO)

12 May 1998

SUBJECT: Authorization for Release of Technical Information, Control Number: **AFRL-PR-ED-TP-1998-078**
T.C. Miller (SPARTA) "Modelling of Plane Strain Interfacial Fracture in Incompressible Materials"

(Statement A)

Modelling of Plane Strain Interfacial Fracture in Incompressible Materials

T. C. Miller
Air Force Research Laboratory, 10 East Saturn Boulevard,
Edwards Air Force Base, California 93524
(805) 275-5323, FAX (805) 275-5435

ABSTRACT

Numerical modelling of a photoelastic experiment is discussed. The experiment examined incompressible materials under plane strain conditions, which results in a simplified analysis due to a vanishing of the bimaterial parameter. The photoelastic experiment used the stress freezing method to determine near tip stresses in interfacial cracks in bimaterial specimens. Different crack orientations were used to produce different mode mixities. Photoelastic fringe patterns were analyzed to determine the magnitude and phase angle of the complex stress intensity factor. These experiments were modeled using a finite element analysis to determine the field variables near the tips of the interfacial cracks. Magnitudes of the complex stress intensity factors are found from J integral values, derived using the domain integral approach, and the phase angles are determined using extrapolation of the bond line traction data to $r = 0$. The results show that this approach is a useful way to characterize completely the complex stress intensity factor in incompressible linear elastic bimaterial combinations under plane strain conditions.

(Keywords: interface, fracture, defects)

INTRODUCTION

The solution of the general case of an interfacial crack lying between two linear elastic isotropic materials was first introduced by Williams in 1959[1]. This boundary value problem was

solved by determining the eigenvalues for the characteristic equation, resulting in an infinite series of eigenvalues with imaginary parts related to the material properties of the two materials. The imaginary component, ϵ, is an inherent part of the field equations, and causes a number of controversies relating to inherent mode mixity, stress oscillation, and predictions of crack face interpenetration[2,3]. Later works attempted to explain these discrepancies[4,5]; however, in a large class of problems these contradictions are predicted only in regions very close to the crack tip and are not significant[2]. Other works presented after Williams' showed that other eigenvalues existed and solved the problem using alternate methods, such as the complex variables formulation of Muskhelishvili. Greater detail is provided in several sources[2,3].

A subset of the general interfacial fracture problem is one in which both materials are incompressible and plane strain conditions exist. In this case, the imaginary part of the complex eigenvalues vanishes, and the mechanics of the crack are analogous to those of a mixed-mode crack in a homogenous material[6,7]. This set of problems includes that of an interfacial crack lying between solid rocket propellant and a rubber liner. To investigate the propellant-liner relationship, a set of photoelastic experiments was performed that also used incompressible materials[6,8].

In previous developments, the stress intensity factor in a photoelastic material was found using the set of isochromatic fringe loops near the tip of the crack. The location of the point along each fringe that was farthest from the crack tip was determined; this set of coordinate data was used to determine the stress intensity factor by extrapolating the data to $r = 0$. This technique was developed for mode I and for mixed-mode loading[9]; the latter was used for the

photoelastic experiments discussed here[6]. Because of the zero valued bimaterial parameter $\underline{\epsilon}$, the presence of two materials provides no additional complications when using this procedure.

The photoelastic experiments used single edge notched tension specimens that incorporated different crack orientations to produce different mode mixities. For these types of specimen and boundary conditions, an approximate analytical solution could be constructed[6]. However, more complex geometries preclude the use of an analytical expression for stress intensity factor calculations. Also, many bimaterial combinations cannot be analyzed using analogous photoelastic materials without ignoring important features of the material behavior. In such cases, developing numerical models may confirm experimental results and help extend the predictive capabilities of the research. It is with this goal that the numerical models featured here have been developed. These models simulate the photoelastic tests so that the evaluation of stress intensity factor magnitudes and phase angles from numerical models can be assessed. A similar method will be used in the study of incompressible bimaterial combinations related to solid rocket motor design.

THEORY

In general, an interfacial crack between two isotropic linear elastic materials will be characterized by a bimaterial parameter $\underline{\epsilon}$[2,3]:

$$\epsilon = \frac{1}{2\pi} Ln\left(\frac{1-\beta}{1+\beta}\right)$$

$$\beta = \frac{\mu_1(\kappa_2 - 1) - \mu_2(\kappa_1 - 1)}{\mu_1(\kappa_2 + 1) + \mu_2(\kappa_1 + 1)} \qquad (1)$$

Here β is one of the two Dundurs' elastic mismatch parameters, μ is the shear modulus, ν is Poisson's ratio, and $\kappa = (3 - \nu) / (1 + \nu)$ in plane stress and $(3 - 4\nu)$ in plane strain. The subscripts are used to index the two materials. In a region near the crack tip, the higher order terms are negligible and the field expressions depend only on the singular terms[10]:

$$\sigma_{pq} = \frac{1}{\sqrt{2\pi r}} \{ Re(\boldsymbol{K} r^{i\epsilon}) \Sigma^{I}_{pq}(\theta) + Im(\boldsymbol{K} r^{i\epsilon}) \Sigma^{II}_{pq}(\theta) \} \qquad (2)$$

Here the two $\underset{\sim}{\Sigma}$ functions characterize the angular variations of the near tip field. Because in-plane tensile and shear loading are coupled, the parameter $\underset{\sim}{K}$ characterizes the combination of these two effects as a complex stress intensity factor. The inherent mode mixity is manifested in the expression for the traction along the interface, derived from eqn (2) by letting $\theta = 0$[2,3]:

$$(\sigma_{yy} + i\sigma_{xy})_{\theta=0} = \frac{\boldsymbol{K} r^{i\epsilon}}{\sqrt{2\pi r}} = \frac{\boldsymbol{K}}{\sqrt{2\pi r}} [\cos(\epsilon Lnr) + i\sin(\epsilon Lnr)] \qquad (3)$$

The complex stress intensity factor $\underset{\sim}{K} = K_1 + i K_2 = Ke^{i\Psi}$ depends on the geometry, loads, stress state, and materials. Inspection of eqn (3) shows that the bond line traction ratio $(\sigma_{xy} / \sigma_{yy})_{\theta=0}$ varies with distance from the crack tip. In a region near the crack tip, the phase angles of the left-hand and right-hand sides of eqn (3) differ by ϵ Ln r:

$$\tan^{-1}[(\sigma_{xy}/\sigma_{yy})_{\theta=0}] = \tan^{-1}[K_2/K_1] + \epsilon Lnr \qquad (4)$$

The magnitude of $\underset{\sim}{K}$ is related to J, the contour integral, through[2]:

$$J = \frac{(c_1 + c_2) |\boldsymbol{K}|^2}{16 \cosh^2(\pi\epsilon)} \qquad (5)$$

Here $c_p = 4(1 - \nu_p) / \mu_p$ in plane strain and $4 / (\mu_p(1 + \nu_p))$ in plane stress. Equations (1-5) show that the presence of the nonzero bimaterial parameter ϵ causes complexities not present in the consideration of homogeneous materials. However, in the special case where both materials are incompressible and plane strain conditions prevail, then $\nu_1 = \nu_2 = ½$ and $\kappa_p = (3 - 4\nu_p)$; substitution into eqn (1) shows that $\beta = \epsilon = 0$ in these circumstances. Introducing $\epsilon = 0$ into eqns (3-5) gives simplified expressions for the degenerate case[6,7]:*

$$(\sigma_{yy} + i\sigma_{xy})_{\theta=0} = \frac{K}{\sqrt{2\pi r}} \tag{6}$$

$$\Psi \equiv \tan^{-1}(K_2/K_1) = \tan^{-1}[(\sigma_{xy}/\sigma_{yy})_{\theta=0}] \tag{7}$$

$$J = \frac{|K|^2}{\overline{E}^*}, \quad \frac{1}{\overline{E}^*} = \frac{1}{2}\left[\frac{1}{\overline{E}_1} + \frac{1}{\overline{E}_2}\right], \quad \overline{E}_1 = \frac{E_1}{1 - \nu_1^2}, \quad \overline{E}_2 = \frac{E_2}{1 - \nu_2^2} \tag{8}$$

The phase angle of the complex stress intensity factor is shown here as Ψ and the effective plane strain elastic modulus $\overline{E}^*$ depends on the plane strain elastic moduli of the two materials. Equations (6-8) show that the solution for an interfacial crack in an incompressible bimaterial pair under plane strain conditions is analogous to that of a homogeneous material with

---

* Because $\nu_1 = \nu_2 = 1/2$, additional simplifications could be made to eqn (8), but it has been presented as shown to preserve the meaning of the parameters.

mixed-mode loading. The ratios (K_2 / K_1) and $(\sigma_{xy} / \sigma_{yy})_{\theta=0}$ are equal in the near tip region, and J and $\underset{\sim}{K}$ are related through a modulus parameter. The additional complexities of stress oscillations, inherent mode mixity, and crack face interpenetration are no longer present.

In the photoelastic experiment, mode mixity was varied by maintaining the vertical loading direction while testing specimens that have different crack orientations. Denoting the angle the crack makes with respect to the mode I loading orientation by Γ, the photoelastic experiments used specimens with crack orientations of $\Gamma = 0°$, 15°, 30°, and 45°. For $\Gamma = 0°$ (mode I loading), the stress intensity factor phase angle equals zero. The mode mixity and phase angle of $\underset{\sim}{K}$ increase in an approximately linear way with increases in Γ[6,8].

DISCUSSION

Figure 1 shows a representative specimen modelled using finite element analysis[6,8]. The set of investigations on which the numerical models is based used a photoelastic polymer, araldite, loaded above its stress freezing temperature of 116° C. The second material is composed of araldite and aluminum powder, so that the two materials have moduli of 18.6 and 36.9 MPa, respectively, above the stress freezing temperature. The latter material is opaque due to the introduction of the aluminum powder, so that photoelastic fringe data is only available for the upper half of each specimen. Above the stress freezing temperature, both materials are incompressible. The two materials were bonded together using a thin layer (less than 0.5 mm) of photoelastic adhesive. The material properties of the adhesive layer were similar to that of the araldite-aluminum; later work confirmed that the presence of a thin adhesive layer causes no significant changes in the relationship between the loads and the complex stress intensity factor[11].

To simulate cracks, notches were machined along the interfaces to a depth of 9.5 mm. Loading was accomplished using freely rotation aluminum grips to which the specimens were bonded, and photoelastic fringe patterns of the loaded specimens were recorded for analysis[7,8].

The complex stress intensity factor was analyzed using fringe loop data from the araldite portion of the specimens. The fringe orders and locations of the maximum radii of the fringe loops near the crack tip were recorded. By extrapolating the data to the crack tip, the complex stress intensity factor can be evaluated. This method overestimated the value of applied $\underline{K}$ for the smaller crack angles because of the influence of residual stresses and machining stresses on the fringe patterns. An analytical model was developed that modified predictions for an edge cracked geometry with finite width effects and notch effects. The experimental results shown in this work are the results of analysis of stress frozen slices taken from the mid-thickness of the specimens so that the data from the experiment represents plane strain conditions[6,8].

Figure 1 shows a typical finite element mesh. Eight-noded quadrilateral elements are used throughout the mesh. Quarter point elements surround the crack tip in a spider web formation as shown in *Figure 2*. The boundary conditions were vertical displacements applied at the outside middle nodes of the aluminum grips (see *Figure 1*). This type of loading closely resembled the pin loading of the actual specimens; rotation at the grips significantly affects the mode mixity at the crack tip.

One complication that arises in the modelling of elastic incompressible materials is the indeterminacy of conventional finite element formulations. Typically, a finite element formulation solves for the displacement components at the nodes in the mesh. The solution will be the configuration that minimizes the potential energy of the mesh, and, in the approximate

sense, the potential energy of the continuum that the mesh represents. The strains and stresses are derived from the nodal displacements using shape functions and constitutive relationships. Usually, a single set of displacements, strains, and stresses minimizes the potential energy of the mesh. However, with incompressible materials, addition of an arbitrary pressure term yields another solution that minimizes the potential energy, so that there are an infinite number of solutions. To resolve this dilemma, the finite element problem is formulated with the hydrostatic component of stress as an additional solution variable. For the eight-noded quadrilateral elements used here, this resulted in three additional degrees of freedom per element: a constant term and linear variations in two orthogonal directions. The resulting mixed formulation avoids the static indeterminacy associated with purely displacement-based formulations[12-14].

The results for each specimen include an estimate of the J integral based on a domain integral approach. To implement this approach, two concentric contours are described that begin on the lower crack face and end on the upper one. The J integral for the inner contour may be restated as an integral involving both contours by using a smooth weighting function[15,16]:

$$J = \int_C (\sigma_{ij} \frac{\partial u_i}{\partial x_1} - w\delta_{1j})\, m_j q_1 \, dC \qquad (10)$$

Here the closed contour C is composed of four contours: C_{inner}, the inner contour; C_{outer}, the outer contour, C_{upper}, the portion of the upper crack face (see *Figure 3*), and C_{lower}, the corresponding portion of the lower crack face. Also, w is the strain energy density, m_j is the jth component of the normal pointing away from the enclosed area, and q_1 is the x_1 component of a certain smoothing function, $\tilde{q}$. The above equation can be converted to an equivalent area integral using the Gauss divergence theorem, giving:

$$J = \int_A \left(\sigma_{ij} \frac{\partial u_i}{\partial x_1} - w\delta_{1j} \right) \frac{\partial q_1}{\partial x_j} \, dA \qquad (11)$$

Here A is the area enclosed by the contours. In practice, the inner contour is allowed to shrink onto the crack tip, the outer contour extends along the edges of the quadrilateral elements, and the area integral is approximated using Gauss quadrature formulas and values for the field variables evaluated at the integration points for each element[16,17]. A method for evaluating J for general interfacial cracks in bimaterials is given by Shih and Asaro, and allow for separation of the energy contributions and determination of K_1 and K_2 using an interaction energy release rate[16]. For the degenerate case discussed here, a simpler methodology can be used to determine the overall energy release rate[15]. The domain integral method of estimating J works well with finite element methods and provides for a robust determination of J that is not sensitive to mesh construction and that does not require highly accurate stress approximations very near to the crack tip. Also, many finite element software programs have built-in algorithms for the determination of the J integral in this manner. The J integral value was used with eqn (8) to calculate the magnitude, K, of the complex stress intensity factor.

Accurate evaluation of the phase angle, Ψ, is then required. Equations (6) and (7) show that the arctangent of the traction ratio σ_{xy}/σ_{yy} along the bond line is equal to Ψ in the near tip region. Using curve fitting techniques, $\tan^{-1}[(\sigma_{xy}/\sigma_{yy})_{\theta=0}]$ can be evaluated as $r \to 0$ and taken as an approximation of Ψ (for the work performed here, a cubic polynomial was used). One problem with this method is that inaccuracies in the stress components caused by high gradients near the crack tip make extrapolation of $(\sigma_{xy}/\sigma_{yy})_{\theta=0}$ to $r = 0$ difficult. An unrefined mesh that

incorporates only a few quarter point elements will exhibit excessive scatter in $\tan^{-1}[(\sigma_{xy}/\sigma_{yy})_{\theta=0}]$ as $r \to 0$, so that this regression technique is unfeasible. This method can be implemented, however, with a more refined mesh, such as the one used here, which incorporates approximately 30 quarter point elements (the number differs for the various crack geometries considered).

The stresses in a finite element formulation are typically found using derivatives of displacement fields based on nodal displacements. Consequently, results for stresses are generally less accurate than displacements in any finite element solution. This dictates that, when possible, extrapolation techniques should be applied to displacements rather than stresses. A method analogous to the stress-based extrapolation technique exists for relative crack face displacements[10,18]. However, this method requires that the two crack faces be initially coincident, so that this technique cannot be easily applied to the current geometry, which incorporates crack faces with finite separation.

In this work, J integral values were used to evaluate K, and bond line traction data was used to determine Ψ, the phase angle of K. Results are presented and compared with the photoelasticity results next.

RESULTS

Figure 4 shows a set of representative contour plots; the plots are for a crack orientation of 45°. The relative size of the two sets of fringe loops is caused by mismatch of the two elastic moduli; the shape of the σ_{yy} and σ_{xy} contours remains invariant with respect to mode mixity. Other stress variables, however, such as the maximum in-plane stress, are strong functions of mode mixity. *Table 1* summarizes the results for both the magnitude and phase of K. Experimental and computational results agreed well. With the $\Gamma = 0°$ and $\Gamma = 15°$ specimens, the

photoelastic results were high due to the effect previously mentioned: residual and machining stresses incorporated into the specimen during fabrication influence the gradient of the fringe patterns in the vertical direction, and this gradient is used in the determination of $\underset{\sim}{K}$.

Table 1 also shows the phase angle results. The worst discrepancy between the numerical and experimental results was for the $\Gamma = 45°$ bimaterial specimen, in which case the values differed by 4.2°. This is accurate enough for most applications, however, if necessary, other methods may be used to obtain additional improvements in accuracy of phase angle determination[16,17]. However, the method shown above is often preferable because of its simplicity compared with other procedures.

CONCLUSIONS

The fracture mechanics of interfacial cracks in incompressible bimaterials subject to plane strain conditions closely resembles those for homogeneous materials subject to mixed-mode loading. Static indeterminacy can cause inaccuracies unless a mixed formulation is used. Numerical modelling can be used to characterize the complex stress intensity factors for various specimen geometries. The magnitude of $\underset{\sim}{K}$ can be evaluated from J integral calculations, and the phase angle of $\underset{\sim}{K}$ can be determined by extrapolating field variables such as the bond line traction data. Mesh refinements should include numerous quarter point elements near the crack tip so that phase angles can be evaluated using extrapolation of bond line traction data.

ACKNOWLEDGMENTS

The author would like to gratefully acknowledge the support of the Air Force Research Laboratory and the collaborative efforts of Dr. C. W. Smith of Virginia Polytechnic Institute and State University for the experimental data and analysis used in this study.

REFERENCES

1 Williams, M.L. The Stresses around a Fault or Crack in Dissimilar Media. *Bulletin of the Seismological Society of America*, 1959, **49**, 199-204.

2 Rice, J.R. Elastic Fracture Mechanics Concepts for Interfacial Cracks. *J. Appl. Mech.*, 1988, **55**, 98-103.

3 Suo, Z. Mechanics of Interface Fracture. Ph.D. dissertation, Harvard University, Cambridge, MA, 1989.

4 Comninou, M. The Interface Crack. *J. Appl. Mech.*, 1977, **44**, 631-636.

5 Evans, A.G. and Hutchinson, J.W. Effects of Non-planarity on the Mixed Mode Fracture Resistance of Bimaterial Interfaces. *Acta Metallurgica*, 1989, **37**, 909-916.

6 Smith, C.W., Finlayson, E.F. and Liu, C.T. A Method for Eavaluating Stress Intensity Distribution for Cracks in Rocket Motor Bondlines. *Eng. Frac. Mech.*, 1997, **58**, 97-105.

7 Hutchinson, J.W. and Suo, Z. Mixed Mode Cracking in Layered Materials. In *Advances in Applied Mechanics*, Academic Press, New York, 1992, pp. 63-91.

8 Finlayson, E.F. Stress Intensity Factor Distributions in Bimaterial Systems - a Three-Dimensional Photoelastic Investigation. Ph.D. dissertation, Virginia Polytechnic Institute and State University, Blacksburg, VA, 1998.

9 Smith, C.W. and Kobayashi, A.S. Experimental Fracture Mechanics. In *Handbook on Experimental Mechanics*, ed. A.S. Kobayashi. VCH Publishing, Bethel, CT, 1993, pp. 905-968.

10 Rice, J.R., Suo, Z. and Wang, J.S. Mechanics and Thermodynamics of Brittle Interfacial Failure in Bimaterial Systems. In *Metal-Ceramic Interfaces*, eds. M. Ruhle, A.G. Evans, M.F. Ashby and J.P. Hirth. Pergamon Press, New York, 1990, pp. 269-294.

11 Miller, T.C., Adhesive Layer Effects on Interfacial Crack Tip Asymptotic Fields. *Fifth International Conference on Composites Engineering*. Las Vegas, NV, July 1998.

12 *ABAQUS/Standard User's Manual, Version 5.5*, Hibbitt, Karlsson, and Sorenson, Pawtucket, RI, 1995.

13 *ABAQUS Theory Manual, Version 5.5*, Hibbitt, Karlsson, and Sorenson, Pawtucket, RI, 1995.

14 Bathe, K.-J. *Finite Element Procedures*, Prentice-Hall, Inc., Upper Saddle River, NJ, 1996.

15 Anderson, T.L. Fracture Mechanics: Fundamentals and Applications, 1st edn. CRC Press, Boca Raton, FL, 1991.

16 Shih, C.F. and Asaro, R.J. Elastic-Plastic Analysis of Cracks on Bimaterial Interfaces: Part I - Small Scale Yielding. *J. Appl. Mech.*, 1988, **55**, 299-316.

17 Li, F.Z., Shih, C.F. and Needleman, A. A Comparison of Methods for Calculating Energy Release Rates. *Eng. Frac. Mech.*, 1985, **21**, 405-421.

18 Smelser, R.E. Evaluation of Stress Intensity Factors for Bimaterial Bodies Using Numerical Crack Flank Displacement Data. *Int. J. Fracture*, 1979, **15**, 135-143.

Table 1 Comparison of numerical modelling and photoelastic results for stress intensity factors

		magnitudes [kPa $m^{1/2}$]		phase angles [degrees]	
applied stress [kPa]	**crack orientation [deg]**	**computational**	**experimental**	**computational**	**experimental**
60.3	0	15.8	19.0	4.0	0.0
96.5	15	24.0	30.2	11.5	7.8
96.5	30	20.8	20.3	19.5	17.1
48.3	45	7.2	8.3	25.8	30.0

LIST OF FIGURES

LIST OF SYMBOLS

β	Dundur's second elastic mismatch parameter
Γ	crack orientation angle
ϵ	bimaterial parameter
θ	angular orientation (second polar coordinate)
κ	kappa
μ	shear modulus
ν	Poisson's ratio
σ_{ij}	stress tensor component
Ψ	complex stress intensity factor phase angle
$\overline{E}^*$	bimaterial effective plane strain modulus
$\overline{E}_1$, $\overline{E}_2$	plane strain moduli for component materials
J	J integral
$\underset{\sim}{K}$	complex stress intensity factor
K	complex stress intensity factor magnitude
r	radius (first polar coordinate)

(a)

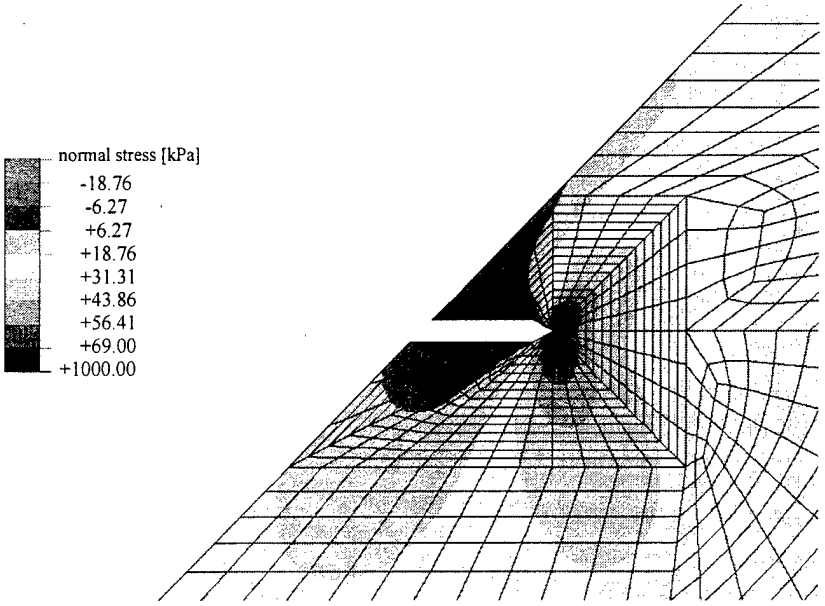
normal stress [kPa]
-18.76
-6.27
+6.27
+18.76
+31.31
+43.86
+56.41
+69.00
+1000.00

(b)

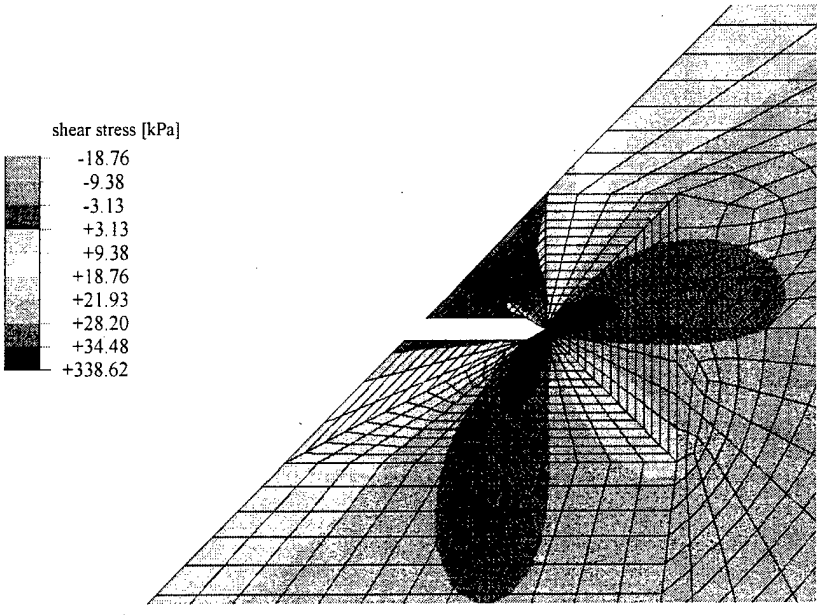
shear stress [kPa]
-18.76
-9.38
-3.13
+3.13
+9.38
+18.76
+21.93
+28.20
+34.48
+338.62

ELSEVIER

Composites: Part B 30 (1999) 291–296

composites
Part B: engineering

Modelling of plane strain interfacial fracture in incompressible materials

T.C. Miller*

Air Force Research Laboratory, 10 East Saturn Boulevard, Edwards Air Force Base, Edwards, CA 93524 USA

Received 24 April 1998; accepted 14 September 1998

Abstract

Numerical modelling of a photoelastic experiment is discussed. The experiment examined incompressible materials under plane strain conditions, which results in a simplified analysis owing to a vanishing of the bimaterial parameter. The photoelastic experiment used the stress freezing method to determine near tip stresses in interfacial cracks in bimaterial specimens. Different crack orientations were used to produce different mode mixities. Photoelastic fringe patterns were analyzed to determine the magnitude and phase angle of the complex stress intensity factor. These experiments were modeled using a finite element analysis to determine the field variables near the tips of the interfacial cracks. Magnitudes of the complex stress intensity factors are found from J integral values, derived using the domain integral approach, and the phase angles are determined using extrapolation of the bond line traction data to $r = 0$. The results show that this approach is a useful way to characterize completely the complex stress intensity factor in incompressible linear elastic bimaterial combinations under plane strain conditions.

Keywords: A. Interface/interphase; B. Fracture; B. Defects

Nomenclature

β	Dundur's second elastic mismatch parameter
Γ	Crack orientation angle
ϵ	Bimaterial parameter
θ	Angular orientation (second polar coordinate)
κ	Kappa
μ	Shear modulus
ν	Poisson's ratio
σ_{ij}	Stress tensor component
Ψ	Complex stress intensity factor phase angle
$\bar{E}*$	Bimaterial effective plane strain modulus
$\bar{E}_1$, $\bar{E}_2$	Plane strain moduli for component materials
J	J integral
$\boldsymbol{K}$	Complex stress intensity factor
K	complex stress intensity factor magnitude
r	radius (first polar coordinate)

1. Introduction

The solution of the general case of an interfacial crack lying between two linear elastic isotropic materials was first introduced by Williams in 1959 [1]. This boundary value problem was solved by determining the eigenvalues for the characteristic equation, resulting in an infinite series of eigenvalues with imaginary parts related to the material properties of the two materials. The imaginary component, ϵ, is an inherent part of the field equations, and causes a number of controversies relating to inherent mode mixity, stress oscillation, and predictions of crack face interpenetration [2,3]. Later works attempted to explain these discrepancies [4,5]; however, in a large class of problems these contradictions are predicted only in regions very close to the crack tip and are not significant [2]. Other works presented after Williams' showed that other eigenvalues existed and solved the problem using alternate methods, such as the complex variables formulation of Muskhelishvili. Greater detail is provided in several sources [2,3].

A subset of the general interfacial fracture problem is one in which both materials are incompressible and plane strain conditions exist. In this case, the imaginary part of the complex eigenvalues vanishes, and the mechanics of the crack are analogous to those of a mixed-mode crack in a homogenous material [6,7]. This set of problems includes that of an interfacial crack lying between solid rocket propellant and a rubber liner. To investigate the propellant–liner relationship, a set of photoelastic experiments was performed that also used incompressible materials [6,8].

In previous developments, the stress intensity factor in a photoelastic material was found using the set of isochromatic fringe loops near the tip of the crack. The location

* Tel.: 001 805 275 5323; fax: 001 805 275 5435.
E-mail address: tim_miller@ple.af.mil (T.C. Miller)

1359-8368/99/$ - see front matter
PII: S1359-8368(98)00064-X

of the point along each fringe that was farthest from the crack tip was determined; this set of coordinate data was used to determine the stress intensity factor by extrapolating the data to $r = 0$. This technique was developed for mode I and for mixed-mode loading [9]; the latter was used for the photoelastic experiments discussed here [6]. Because of the zero valued bimaterial parameter ϵ, the presence of two materials provides no additional complications when using this procedure.

The photoelastic experiments used single edge notched tension specimens that incorporated different crack orientations to produce different mode mixities. For these types of specimen and boundary conditions, an approximate analytical solution could be constructed [6]. However, more complex geometries preclude the use of an analytical expression for stress intensity factor calculations. Also, many bimaterial combinations cannot be analyzed using analogous photoelastic materials without ignoring important features of the material behavior. In such cases, developing numerical models may confirm experimental results and help extend the predictive capabilities of the research. It is with this goal that the numerical models featured here were developed. These models simulate the photoelastic tests so that the evaluation of stress intensity factor magnitudes and phase angles from numerical models can be assessed. A similar method will be used in the study of incompressible bimaterial combinations related to solid rocket motor design.

2. Theory

In general, an interfacial crack between two isotropic linear elastic materials will be characterized by a bimaterial parameter ϵ [2,3].

$$\epsilon = \frac{1}{2\pi}\ln\left(\frac{1-\beta}{1+\beta}\right),\ \beta = \frac{\mu_1(\kappa_2 - 1) - \mu_2(\kappa_1 - 1)}{\mu_1(\kappa_2 + 1) + \mu_2(\kappa_1 + 1)} \tag{1}$$

Here β is one of the two Dundurs' elastic mismatch parameters, μ the shear modulus, ν Poisson's ratio, and $\kappa = (3 - \nu)/(1 + \nu)$ in plane stress and $(3 - 4\nu)$ in plane strain. The subscripts are used to index the two materials. In a region near the crack tip, the higher order terms are negligible and the field expressions depend only on the singular terms [10]:

$$\sigma_{pq} = \frac{1}{\sqrt{2\pi r}}\left\{\mathrm{Re}\left(\boldsymbol{K}r^{i\epsilon}\right)\sum_{pq}^{I}(\theta) + \mathrm{Im}\left(\boldsymbol{K}r^{i\epsilon}\right)\sum_{pq}^{II}(\theta)\right\} \tag{2}$$

Here the two Σ functions characterize the angular variations of the near tip field. Because in-plane tensile and shear loading are coupled, the parameter $\boldsymbol{K}$ characterizes the combination of these two effects as a complex stress intensity factor. The inherent mode mixity is manifested in the expression for the traction along the interface, derived from Eq. (2) by letting $\theta = 0$ [2,3]:

$$\left(\sigma_{yy} + i\sigma_{xy}\right)_{\theta=0} = \frac{\boldsymbol{K}r^{i\epsilon}}{\sqrt{2\pi r}} = \frac{\boldsymbol{K}}{\sqrt{2\pi r}}[\cos(\epsilon \ln r) + i\sin(\epsilon \ln r)] \tag{3}$$

The complex stress intensity factor $\boldsymbol{K} = K_1 + iK_2 = Ke^{i\Psi}$ depends on the geometry, loads, stress state, and materials. Inspection of Eq. (3) shows that the bond line traction ratio $(\sigma_{xy}/\sigma_{yy})_{\theta=0}$ varies with distance from the crack tip. In a region near the crack tip, the phase angles of the left-hand and right-hand sides of Eq. (3) differ by $\epsilon \ln r$:

$$\tan^{-1}\left[\left(\frac{\sigma_{xy}}{\sigma_{yy}}\right)_{\theta=0}\right] = \tan^{-1}\left[\frac{K_2}{K_1}\right] + \epsilon \ln r \tag{4}$$

The magnitude of $\boldsymbol{K}$ is related to J, the contour integral, through [2]:

$$J = \frac{(c_1 + c_2)\,|\boldsymbol{K}|^2}{16\cosh^2(\pi\epsilon)} \tag{5}$$

Here $c_p = 4(1 - \nu_p)/\mu_p$ in plane strain and $4/(\mu_p(1 + \nu_p))$ in plane stress. Eqs. (1)–(5) show that the presence of the nonzero bimaterial parameter ϵ causes complexities not present in the consideration of homogeneous materials. However, in the special case where both materials are incompressible and plane strain conditions prevail, then $\nu_1 = \nu_2 = 1/2$ and $\kappa_p = (3 - 4\nu_p)$; substitution into Eq. (1) shows that $\beta = \epsilon = 0$ in these circumstances. Introducing $\epsilon = 0$ into Eqs. (3)–(5) gives simplified expressions for the degenerate case [6,7][1]:

$$(\sigma_{yy} + i\,\sigma_{xy})_{\theta=0} = \frac{\boldsymbol{K}}{\sqrt{2\pi r}}, \tag{6}$$

$$\Psi \equiv \tan^{-1}\left(\frac{K_2}{K_1}\right) = \tan^{-1}\left[\left(\frac{\sigma_{xy}}{\sigma_{xy}}\right)_{\theta=0}\right] \tag{7}$$

$$J = \frac{|\boldsymbol{K}|^2}{\overline{E^*}},$$
$$\frac{1}{\overline{E^*}} = \frac{1}{2}\left[\frac{1}{\overline{E_1}} + \frac{1}{\overline{E_2}}\right],\ \overline{E_1} = \frac{E_1}{1-\nu_1^2},\ \overline{E_2} = \frac{E_2}{1-\nu_2^2} \tag{8}$$

The phase angle of the complex stress intensity factor is shown here as Ψ and the effective plane strain elastic modulus $\overline{E^*}$ depends on the plane strain elastic moduli of the two materials. Eqs. (6)–(8) show that the solution for an interfacial crack in an incompressible bimaterial pair under plane strain conditions is analogous to that of a homogeneous material with mixed-mode loading. The ratios (K_2/K_1) and $(\sigma_{xy}/\sigma_{yy})_{\theta=0}$ are equal in the near tip region and J and $\mathbf{K}$ are related through a modulus parameter. The additional

[1] Because $\nu_1 = \nu_2 = 1/2$, additional simplifications could be made to Eq. (8), but it has been presented as shown to preserve the meaning of the parameters.

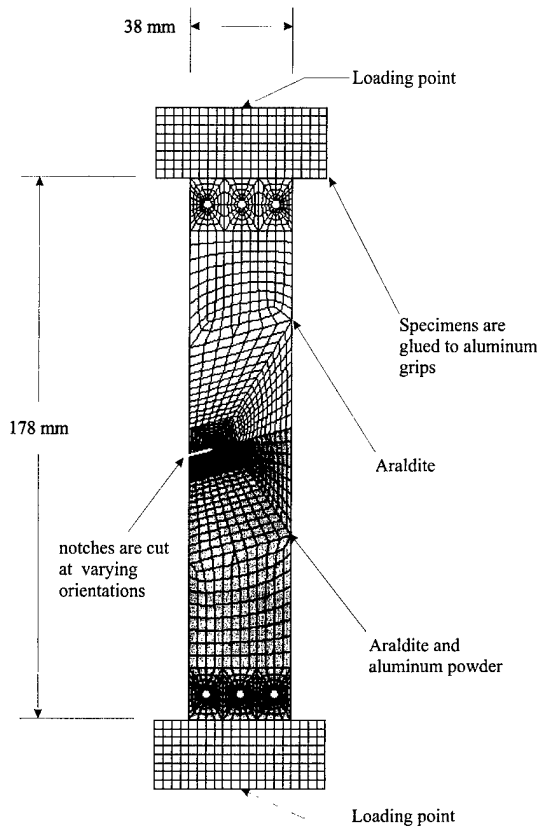

Fig. 1. Typical finite element mesh used in numerical computations (crack orientation = 15 degrees).

complexities of stress oscillations, inherent mode mixity, and crack face interpenetration are no longer present.

In the photoelastic experiment, mode mixity was varied by maintaining the vertical loading direction while testing specimens that have different crack orientations. Denoting the angle the crack makes with respect to the mode I loading orientation by Γ, the photoelastic experiments used specimens with crack orientations of $\Gamma = 0°$, 15°, 30°, and 45°. For $\Gamma = 0°$ (model I loading), the stress intensity factor phase angle equals zero. The mode mixity and phase angle of $\mathbf{K}$ increase in an approximately linear way with increases in Γ [6,8].

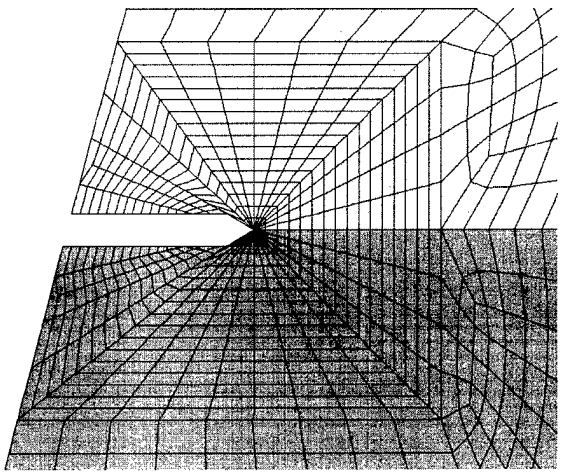

Fig. 2. Detail of finite element mesh near the crack tip (crack orientation = 15 degrees).

3. Discussion

Fig. 1 shows a representative specimen modelled using finite element analysis [6,8]. The set of investigations on which the numerical models is based used a photoelastic polymer, araldite, loaded above its stress freezing temperature of 116°C. The second material is composed of araldite and aluminum powder, so that the two materials have moduli of 18.6 and 36.9 MPa, respectively, above the stress freezing temperature. The latter material is opaque because of the introduction of the aluminum powder, so that photoelastic fringe data is only available for the upper half of each specimen. Above the stress freezing temperature, both materials are incompressible. The two materials were bonded together using a thin layer (less than 0.5 mm) of photoelastic adhesive. The material properties of the adhesive layer were similar to that of the araldite–aluminum; later work confirmed that the presence of a thin adhesive layer causes no significant changes in the relationship between the loads and the complex stress intensity factor [11].

To simulate cracks, notches were machined along the interfaces to a depth of 9.5 mm. Loading was accomplished using freely rotating aluminum grips to which the specimens were bonded, and photoelastic fringe patterns of the loaded specimens were recorded for analysis [7,8].

The complex stress intensity factor was analyzed using fringe loop data from the araldite portion of the specimens. The fringe orders and locations of the maximum radii of the fringe loops near the crack tip were recorded. By extrapolating the data to the crack tip, the complex stress intensity factor can be evaluated. This method overestimated the value of applied K for the smaller crack angles because of the influence of residual stresses and machining stresses on the fringe patterns. An analytical model was developed that modified predictions for an edge cracked geometry with finite width effects and notch effects. The experimental results shown in this work are the results of analysis of stress frozen slices taken from the mid-thickness of the specimens so that the data from the experiment represents plane strain conditions [6,8].

Fig. 1 shows a typical finite element mesh. Eight-noded quadrilateral elements are used throughout the mesh. Quarter point elements surround the crack tip in a spider web formation as shown in Fig. 2. The boundary conditions were vertical displacements applied at the outside middle nodes of the aluminum grips (see Fig. 1). This type of loading closely resembled the pin loading of the actual specimens;

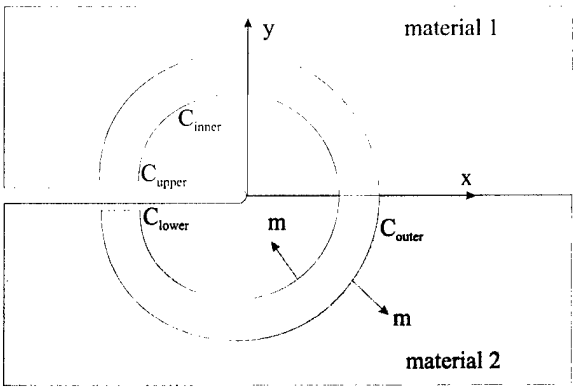

Fig. 3. Evaluation of J integral using domain integral method.

rotation at the grips significantly affects the mode mixity at the crack tip.

One complication that arises in the modelling of elastic incompressible materials is the indeterminacy of conventional finite element formulations. Typically, a finite element formulation solves for the displacement components at the nodes in the mesh. The solution will be the configuration that minimizes the potential energy of the mesh, and, in the approximate sense, the potential energy of the continuum that the mesh represents. The strains and stresses are derived from the nodal displacements using shape functions and constitutive relationships. Usually, a single set of displacements, strains, and stresses minimizes the potential energy of the mesh. However, with incompressible materials, addition of an arbitrary pressure term yields another solution that minimizes the potential energy, so that there are an infinite number of solutions. To resolve this dilemma, the finite element problem is formulated with the hydrostatic component of stress as an additional solution variable. For the eight-noded quadrilateral elements used here, this resulted in three additional degrees of freedom pet element: a constant term and linear variations in two orthogonal directions. The resulting mixed formulation avoids the static indeterminacy associated with purely displacement-based formulations [12–14].

The results for each specimen include an estimate of the J integral based on a domain integral approach. To implement this approach, two concentric contours are described that begin on the lower crack face and end on the upper one. The J integral for the inner contour may be restated as an integral involving both contours by using a smooth weighting function [15,16].

$$J = \int_c \left(\sigma_{ij}\frac{\partial u_i}{\partial x_1} - w\delta_{1j}\right) m_j q_1 \, \mathrm{d}c \tag{9}$$

Here the closed contour C is composed of four contours: C_{inner}, the inner contour, C_{outer}, the outer contour, C_{upper}, the portion of the upper crack face (see Fig. 3) and C_{lower}, the corresponding portion of the lower crack face. Also, w is the strain energy density, m_j is the jth component of the normal pointing away from the enclosed area, and q_1 is the x_1 component of a certain smoothing function, q. The above equation can be converted to an equivalent area integral using the Gauss divergence theorem, giving:

$$J = \int_A \left(\sigma_{ij}\frac{\partial u_i}{\partial x_1} - w\delta_{1j}\right)\frac{\partial q_1}{\partial x_j} \, \mathrm{d}A \tag{10}$$

Here A is the area enclosed by the contours. In practice, the inner contour is allowed to shrink onto the crack tip, the outer contour extends along the edges of the quadrilateral elements, and the area integral is approximated using Gauss quadrature formulas and values for the field variables evaluated at the integration points for each element [16,17]. A method for evaluating J for general interfacial cracks in bimaterials is given by Shih and Asaro, and allows for separation of the energy contributions and determination of K_1 and K_2 using an interaction energy release rate [16]. For the degenerate case discussed here, a simpler methodology can be used to determine the overall energy release rate [15]. The domain integral method of estimating J works well with finite element methods and provides for a robust determination of J that is not sensitive to mesh construction and that does not require highly accurate stress approximations very near to the crack tip. Also, many finite element software programs have built-in algorithms for the determination of the J integral in this manner. The J integral value was used with Eq. (8) to calculate the magnitude, K, of the complex stress intensity factor.

Accurate evaluation of the phase angle, Ψ, is then required. Eqs. (6) and (7) show that the arctangent of the traction ratio σ_{xy}/σ_{yy} along the bond line is equal to Ψ in the near tip region. Using curve fitting techniques, $\tan^{-1}[(\sigma_{xy}/\sigma_{yy})_{\theta=0}]$ can be evaluated as $r \to 0$ and taken as an approximation of Ψ (for the work performed here, a cubic polynomial was used). One problem with this method is that inaccuracies in the stress components caused by high gradients near the crack tip make extrapolation of $(\sigma_{xy}/\sigma_{yy})_{\theta=0}$ to $r = 0$ difficult. An unrefined mesh that incorporates only a few quarter point elements will exhibit excessive scatter in $\tan^{-1}[(\sigma_{xy}/\sigma_{yy})_{\theta=0}]$ as $r \to 0$, so that this regression technique is unfeasible. This method can be implemented, however, with a more refined mesh, such as the one used here, which incorporates approximately 30 quarter point elements (the number differs for the various crack geometries considered).

The stresses in a finite element formulation are typically found using derivatives of displacement fields based on nodal displacements. Consequently, results for stresses are generally less accurate than displacements in any finite element solution. This dictates that, when possible, extrapolation techniques should be applied to displacements rather than stresses. A method analogous to the stress-based extrapolation technique exists for relative crack face displacements [10,18]. However, this method requires that the two crack faces be initially coincident, so that this technique cannot be easily applied to the

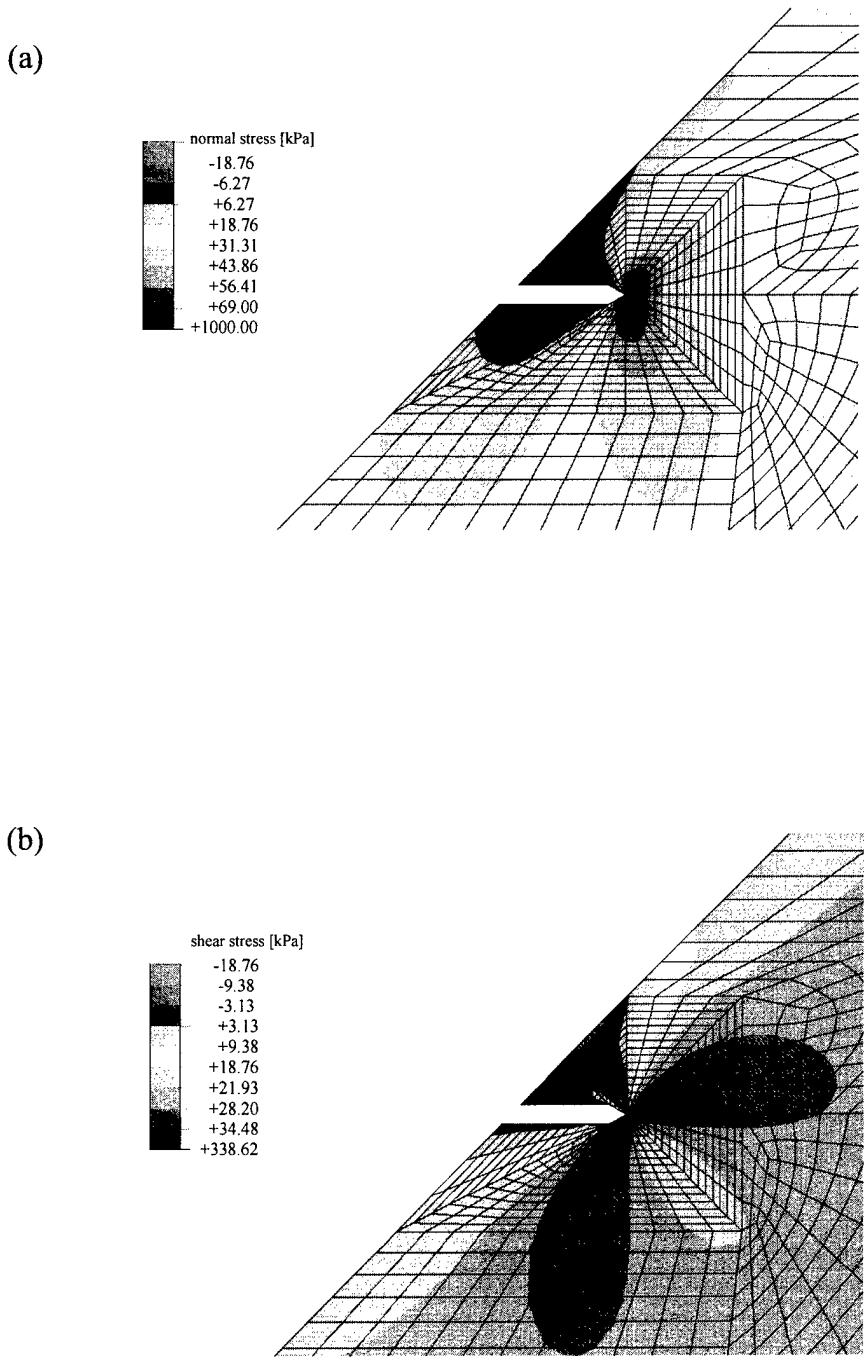

Fig. 4. Contour plots of normal and shear stresses near the crack tip (bimaterial specimen, crack orientation = 45 degrees).

Table 1
Comparison of numerical modelling and photoelastic results for stress intensity factors

Applied stress (kPa)	Crack orientation (degrees)	Magnitudes (kPa $m^{1/2}$)		Phase angles (degrees)	
		Computational	Experimental	Computational	Experimental
60.3	0	15.8	19.0	4.0	0.0
96.5	15	24.0	30.2	11.5	7.8
96.5	30	20.8	20.3	19.5	17.1
48.3	45	7.2	8.3	25.8	30.0

current geometry, which incorporates crack faces with finite separation.

In this work, J integral values were used to evaluate K, and bond line traction data was used to determine Ψ, the phase angle of **K**. Results are presented and compared with the photoelasticity results next.

4. Results

Fig. 4 shows a set of representative contour plots; the plots are for a crack orientation of 45°. The relative size of the two sets of fringe loops is caused by mismatch of the two elastic moduli; the shape of the σ_{yy} and σ_{xy} contours remains invariant with respect to mode mixity. Other stress variables, however, such as the maximum in-plane stress, are strong functions of mode mixity. Table 1 summarizes the results for both the magnitude and phase of **K**. Experimental and computational results agreed well. With the $\Gamma = 0°$ and $\Gamma = 15°$ specimens, the photoelastic results were high because of the effect previously mentioned: residual and machining stresses incorporated into the specimen during fabrication influence the gradient of the fringe patterns in the vertical direction, and this gradient is used in the determination of **K**.

Table 1 also shows the phase angle results. The worst discrepancy between the numerical and experimental results was for the $\Gamma = 45°$ bimaterial specimen, in which case the values differed by 4.2°. This is accurate enough for most applications, however, if necessary, other methods may be used to obtain additional improvements in accuracy of phase angle determination [16,17]. However, the method shown above is often preferable because of its simplicity compared with other procedures.

5. Conclusions

The fracture mechanics of interfacial cracks in incompressible bimaterials subject to plane strain conditions closely resembles those for homogeneous materials subject to mixed-mode loading. Static indeterminacy can cause inaccuracies unless a mixed formulation is used. Numerical modelling can be used to characterize the complex stress intensity factors for various specimen geometries. The magnitude of **K** can be evaluated from J integral calculations, and the phase angle of **K** can be determined by extrapolating field variables such as the bond line traction data. Mesh refinements should include numerous quarter point elements near the crack tip so that phase angles can be evaluated using extrapolation of bond line traction data.

Acknowledgements

The author would like to gratefully acknowledge the support of the Air Force Research Laboratory and the collaborative efforts of Dr. C.W. Smith of Virginia Polytechnic Institute and State University for the experimental data and analysis used in this study.

References

[1] Williams ML. The stresses around a fault or crack in dissimilar media. Bull Seismolog Soc America 1959;49:199–204.
[2] Rice JR. Elastic fracture mechanics concepts for interfacial cracks. J Appl Mech 1988;55:98–103.
[3] Suo Z. Mechanics of interface fracture. Ph.D. dissertation, Harvard University, Cambridge, MA, 1989.
[4] Comninou M. The interface crack. J Appl Mech 1977;44:631–636.
[5] Evans AG, Hutchinson JW. Effects of non-planarity on the mixed mode fracture resistance of bimaterial interfaces. Acta Metallurgica 1989;37:909–916.
[6] Smith CW, Finlayson EF, Liu CT. A method for evaluating stress intensity distribution for cracks in rocket motor bondlines. Eng Frac Mech 1997;58:97–105.
[7] Hutchinson JW, Suo Z. Mixed mode cracking in layered materials. Advances in Applied Mechanics. New York: Academic Press, 1992 pp. 63–91.
[8] Finlayson, EF. Stress intensity factor distributions in bimaterial systems – a three-dimensional photoelastic investigation. Ph.D. dissertation, Virginia Polytechnic Institute and State University, Blacksburg, VA, 1998.
[9] Smith CW, Kobayashi AS. Experimental fracture mechanics. In: Kobayashi AS, editor. Handbook on Experimental Mechanics, Bethel, CT: VCH Publishing, 1993. pp. 905.
[10] Rice JR, Suo Z, Wang JS. Mechanics and thermodynamics of brittle interfacial failure in bimaterial systems. In: Ruhle M, Evans AG, Ashby MF, Hirth JP, editors. Metal–Ceramic Interfaces, New York: Pergamon Press, 1990. pp. 269.
[11] Miller, TC, Adhesive layer effects on interfacial crack tip asymptotic fields, Fifth International Conference on Composites Engineering, Las Vegas, NV, July 1998.
[12] ABAQUS/Standard User's Manual, Version 5.5, Hibbitt, Karlsson and Sorenson, Pawtucket, RI, 1995.
[13] ABAQUS Theory Manual, Version 5.5, Hibbitt, Karlsson and Sorenson, Pawtucket, RI, 1995.
[14] Bathe K-J. Finite Element Procedures, Upper Saddle River, NJ: Prentice-Hall Inc, 1996.
[15] Anderson TL. Fracture mechanics: fundamentals and applications, 1. Boca Raton, FL: CRC Press, 1991.
[16] Shih CF, Asaro RJ. Elastic-plastic analysis of cracks on bimaterial interfaces: Part I – Small scale yielding. J Appl Mech 1988;55:299–316.
[17] Li FZ, Shih CF, Needleman AA. A comparison of methods for calculating energy release rates. Eng Frac Mech 1985;21:405–421.
[18] Smelser RE. Evaluation of stress intensity factors for bimaterial bodies using numerical crack Flank displacement data. Int J Fracture 1979;15:135–143.